The International Archives of the Photogrammetry, Remote Sensing and Spatial Information Sciences, Volume XLVIII-1/W3-2023
2nd GEOBENCH Workshop on Evaluation and BENCHmarking of Sensors, Systems and GEOspatial Data
in Photogrammetry and Remote Sensing, 23–24 October 2023, Krakow, Poland

GEOMETRIC PROCESSING OF VERY HIGH-RESOLUTION SATELLITE IMAGERY: QUALITY ASSESSMENT FOR 3D MAPPING NEEDS

E.M. Farella[1], F. Remondino[1], C. Cahalane[2], R. Qin[3], A.M. Loghin[4,5], M. Di Tullio[6], N. Haala[7], J. Mills[8]

[1] 3D Optical Metrology Unit, Bruno Kessler Foundation (FBK), Trento, Italy – Email: (elifarella)(remondino)@fbk.eu

[2] Department of Geography, Rhetoric House, Maynooth University, Co. Kildare, Ireland – Email: conor.cahalane@mu.ie

[3] Geospatial Data Analytics Laboratory, The Ohio State University, Columbus, USA – Email: qin.324@osu.edu

[4] Department of Geodesy and Geoinformation, Technical University of Vienna, Austria – Email: ana-maria.loghin@geo.tuwien.ac.at

[5] Federal Office of Metrology and Surveying (BEV), Vienna, Austria – Email: Ana-Maria.Loghin@bev.gv.at

[6] GMatics, Rome, Italy – Email: marco.ditullio@gmatics.eu

[7] Institute for Photogrammetry, University of Stuttgart, Germany – Email: norbert.haala@ifp.uni-stuttgart.de

[8] School of Engineering, Newcastle University, United Kingdom – Email: jon.mills@newcastle.ac.uk

KEY WORDS: high-resolution satellite images, optical, 3D processing, DSM, NMCAs, mapping

ABSTRACT:
In recent decades, the geospatial domain has benefitted from technological advances in sensors, methodologies, and processing tools to expand capabilities in mapping applications. Airborne techniques (LiDAR and aerial photogrammetry) generally provide most of the data used for this purpose. However, despite the relevant accuracy of these technologies and the high spatial resolution of airborne data, updates are not sufficiently regular due to significant flight costs and logistics. New possibilities to fill this information gap have emerged with the advent of Very High Resolution (VHR) optical satellite images in the early 2000s. In addition to the high temporal resolution of the cost-effective datasets and their sub-meter geometric resolutions, the synoptic coverage is an unprecedented opportunity for mapping remote areas, multi-temporal analyses, updating datasets and disaster management. For all these reasons, VHR satellite imagery is clearly a relevant study for National Mapping and Cadastral Agencies (NMCAs). This work, supported by EuroSDR, summarises a series of experimental analyses carried out over diverse landscapes to explore the potential of VHR imagery for large-scale mapping.

Figure 1. A sample tri-stereo acquisition (Pleaides, 2018) over the Colosseum (Rome, Italy). Panchromatic image resolution: 0.5 m. Viewing directions: forward (left), nadir (middle), and backward (right), near-polar sun-synchronous orbit (694 km).

1. INTRODUCTION

With the advent of very high-resolution (VHR) satellite imagery in the early 2000s, new opportunities have emerged for Earth Observation (EO), monitoring, and mapping (Dowman et al., 2022). Applications of VHR imagery are growing in different sectors, and this trend is expected to continue due to the multiple advantages of these sources.

Although LiDAR and photogrammetric airborne data are still unquestionably preferential sources for most mapping and cadastral applications, we are witnessing increasing performances of VHR satellite sensors (and related geo-products), a large interest in exploring their potential and complementarity, new space initiatives and new opportunities for end-users (Denis et al., 2017). Both traditional active (LiDAR) and passive (photogrammetry) techniques currently provide accurate 3D information on mapped areas, even though these solutions feature limited area coverage and low temporal resolution due to high flight costs and the need for flight permissions. In contrast, the lower spatial resolution of satellite images is compensated for by the extensive area coverage and the short time interval between data capture, leveraging the availability of different sensors and constellations. Examples of commercial VHR satellites are Pleiades 1A/1B, GeoEye-1, WorldView 1-4, SPOT 6/7, GaoJing/SuperView-1, etc. These platforms acquire in continuous or target mode, with irregular imaging configurations, multi-spectral capabilities, a spatial resolution (GSD) from 30 cm to 2 m and a temporal resolution from days to weeks. It is this high temporal resolution capability that makes these data suitable for multiple priority monitoring purposes, for example, in case of hazards and disasters (Poli and Caravaggi, 2013). Furthermore, the use of these data for mapping is an unprecedented opportunity, in particular for developing countries, where aerial flights cannot readily be performed, and current topographic information is generally unavailable (Watson et al., 2022). Stereoscopic or tri-stereo images are normally acquired along-track (Figure 1), although across-track is also possible (Krauss et al., 2019). Along-track triplets are captured by rotating the imaging sensor in forward, nadir, and backward directions, ensuring better coverage and reducing occlusions for 3D reconstruction purposes (Figure 2).

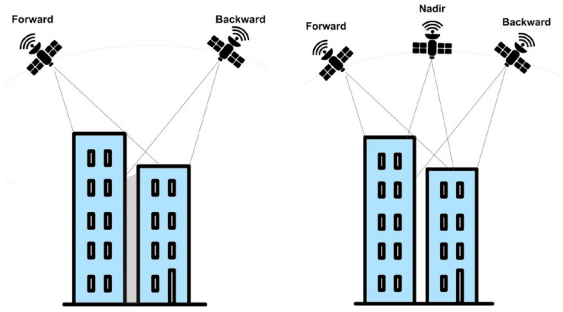

Figure 2. Schematic representation of stereo (left) and tri-stereo (right) acquisition geometry with occluded areas.

1.1 Paper's contribution

The derivation of accurate geospatial products from VHR imagery shows the potential to be a valuable complementary source of geospatial information for National Mapping and Cadastral Agencies (NMCAs). Therefore, the reported research activity, supported by EuroSDR, explores VHR optical satellite imagery for 3D mapping purposes. Through diverse experiments and analyses using a range of datasets and tools (Table 1), the work reports best practices and quality assessments of geospatial products (DSMs, orthophotos, LoD1) traditionally used by NMCAs for their activities.

2. RELATED WORKS

The majority of research dedicated in the last four decades to optical satellite imagery has explored these as 2D datasets and examined the potential of these sources primarily in a spectral context (Qui and Liu, 2022). Scientific production linked to the 3D capabilities of VHR satellite data is a more recent prospect. 3D studies have focussed mainly on optimizing the photogrammetric processing pipeline or applying VHR stereo capabilities to specific sectors (Sirmacek et al., 2012; Barbarella et al., 2017; Loghin et al., 2020; Stylianidis et al., 2020).

The derivation of high-quality geospatial products, mostly Digital Surface Models (DSMs) and orthophotos, primarily depends on the accurate calibration and orientation of the sensor. The relation between the object and image space is expressed with physical (rigorous) or generalized sensor models (Poli and Tautin, 2002). Rational Function Models (RFM), based on Rational Polynomial Coefficients (RPCs), are commonly used as an alternative to physical models for faster and more cost-effective mapping from VHR images (Hu et al., 2004). This improvement of the positioning accuracy of satellite-based data, especially through new methods for RPCs bias correction, has been the point of convergence of several studies (Luong and Wolniewicz, 2005; Fraser et al., 2006; Xiong and Zhang, 2009; Tang et al., 2016; Dong et al, 2020; Marí et al., 2021; Junpeng et al., 2022; Loghin et al., 2022).

Furthermore, various research contributions have been proposed for improving the automatic creation of 3D surface and building models, contributing at different stages of the reconstruction pipeline (Deilami and Hashim, 2011; Poli et al., 2015; Shean et al., 2016; Qin, 2016; Facciolo et al., 2017; Partovi et al., 2019; Perko et al., 2019; Qui, 2019; Rothermel et al., 2020; Breaban et al., 2022; Qin et al., 2022).

Considering the expected growth of this image processing sector, increasingly more tools and algorithms, either conventional (De Franchis et al., 2014; Di Rita et al., 2017; Rupnik et al, 2018) or based on deep learning methods (Stucker et al., 2022; Gao et al., 2023), are available or under development, including those dedicated to the LoD1 and LoD2 building models creation (Gui and Qin, 2021). A fully automatic production of a worldwide accurate DSM is also planned (Lebègue et al., 2020).

Free datasets for VHR optical satellite imagery are rare due to license conditions (Agugiaro et al., 2012; Bosch et al., 2016; Patil et al., 2019). Benchmarking geometric capabilities and product evaluations were presented in Reinartz et al. (2010), Capaldo et al. (2012), Kuschk et al. (2014), Poli et al. (2015) and Aguilar et al. (2019).

3. DATASETS DESCRIPTION

The authors collected diverse stereo and tri-stereo (Figure 3) datasets over urban or vegetated locations to examine the capabilities of VHR satellite optical imagery in supporting NMCAs mapping needs and geo-products derivation. The characteristics of each dataset, the corresponding ground truth data and the processing tools employed are reported in Table 1. In some cases, images acquired from different sensors are available over the same area. The VHR satellite sensors and imagery include:

- GeoEye-1: launched in 2008 and still operational. The sun-synchronous descending mode orbit is at 681 km, with an orbital period of ca 99 minutes. Images are collected at 0.41 m panchromatic and 1.65 m 4-band multi-spectral with a 15.2 km swath. The optical system has a focal length of 13.3 m. The stated geolocation accuracy is 3 m without Ground Control Points (GCPs).
- Pleiades: consists of two satellites, named 1A and 1B, launched respectively in 2011 and 2012, with a sun-synchronous descending mode orbit at an altitude of 694 km. The optical system has a focal length of 12.905 m, delivering 0.5 m panchromatic and 2 m 4-band multi-spectral images with a 20 m swath and a daily revisit interval. The geolocation accuracy is ca 20 m without GCPs, while 1 m is achievable if GCPs are included in the processing.
- WorldView-3: was launched in 2014 and is still functioning. The sun-synchronous descending mode orbit height is at 617 km, with an orbit period of ca 97 minutes. Images are collected at 0.3 m panchromatic, 1.24 m 8-band multi-spectral VNIR, 3.7 m 8-band multi-spectral SWIR and 30m in the CAVIS bands, with 15.2 km swath. The optical system has a focal length of 13.3 m. The declared geolocation accuracy is below 3 m.

Each dataset includes a set of supplier-provided RPCs for the transformation between image and object space.

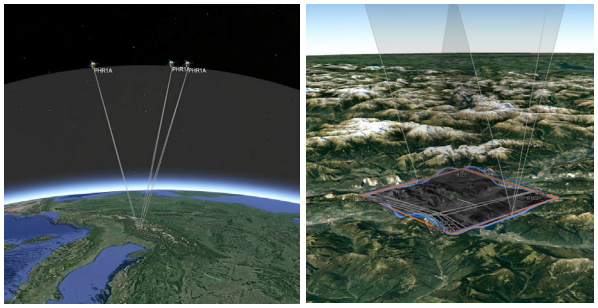

Figure 3: Example of acquisition geometry and coverage area for a Pleiades tri-stereo dataset over Trento (Italy).

Sensor / Satellite	Acquisition date	Type	Location	GSD (m)	Conv. Angle	Ground Truth	RSP	Agisoft Metashape	Erdas Imagine	Trimble Inpho
WorldView3	2017	Stereo	Rome, Italy	0.3	NB 38°	LiDAR (2017) 0.5 m	X	X	X	
GeoEye 1	2018	Triplet	Rome, Italy	0.4	FN 15° NB 14° FB 29°	LiDAR (2017) 0.5 m	X		X	
GeoEye 1	2011	Stereo	Trento, Italy	0.5	FB 30°	LiDAR (2014) 1 m	X		X	
Pleiades (1A)	2012	Triplet	Trento, Italy	0.7	FN 5° NB 27° FB 33°	LiDAR (2014) 1 m	X		X	
Pleiades (1B)	2017	Triplet	Dublin, Ireland	0.5	FN 6° NB 18° FB 24°	Photog. (2018) 0.25 m	X	X	X	
Pleiades (1B)	2017	Triplet	Allentsteig, Austria	0.5	FN 14° NB 14° FN 25°	LiDAR (2022) 1 m	X	X	X	X
WorldView3	2018	Triplet	Allentsteig, Austria	0.5	FN 13° NB 13° FB 25°	LiDAR (2022) 1 m	X		X	X

Table 1. Dataset characteristics and processing tools considered in this benchmark. Tools include commercial solutions (Agisoft Metashape, ERDAS Imagine, Trimble Inpho) and the RPC Stereo Processor tool (hereafter named RSP) by Qin (2016), awarded at the 2022 ISPRS CATCON contest and free for academic use. The convergence angles express the acquisition geometry between an image pair (stereo case) or the Forward-Nadir (FN), Nadir-Backward (NB) and the Forward-Backward images (triple-stereo mode).

4. QUESTIONNAIRE

In the first phase of the project, a questionnaire was submitted to several stakeholders involved in different geospatial data production and analysis activities. The aim was to gain a clearer picture of current needs in the geospatial domain and the level of knowledge and practice with VHR imageries in the sector. The questionnaire was filled in mainly by NMCAs, research institutions and universities. Most participants declared (Figures 4-7) familiarity with the use of VHR satellite data (especially orthophotos, but also point clouds, raw imagery, multispectral and PAN images). While "high temporal resolution" and "more affordable costs" are recognized as greater values of these sources compared to traditional airborne techniques, the "lower spatial resolution" emerged as the main concern. The production of DSMs was, instead, the application of most interest for the participants.

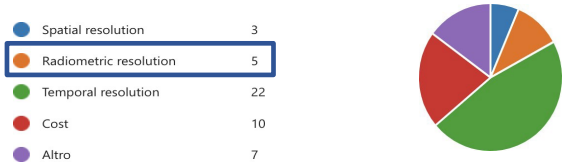

Figure 4. Summarizing chart: advantages of stereo and tri-stereo images with respect to the airborne techniques.

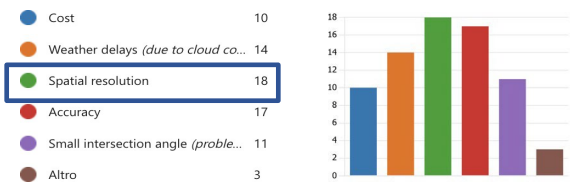

Figure 5. Summarizing chart: disadvantages of stereo and tri-stereo images with respect to the airborne techniques.

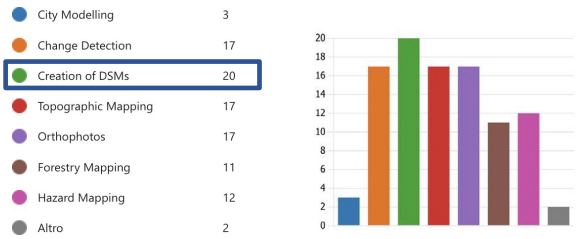

Figure 6. Summarizing chart: suitable applications of stereo and tri-stereo satellite imagery.

Figure 7. Summarizing chart: satellite-derived data characteristics ranked for importance.

5. DATA PROCESSING AND GEOMETRIC ANALYSES

Different experimental analyses were conducted with the available datasets (Table 1) to produce typical geospatial products and report best practices for NMCAs. In the following sections, specific tests are reported: they are related to RPC bias compensation, DSM generation, 3D building model creation and reachable accuracy.

5.1 Stereo vs tri-stereo reconstruction (Rome datasets)

The Rome datasets have two image acquisition geometries (stereo and tri-stereo pairs) and resolutions (30 cm for WorldView-3 and 40 cm for GeoEye-1). The derived DSMs (at 0.5 m, Figure 8) were compared with the available ground truth LiDAR data by computing the vertical residuals at each corresponding point as raster differences (Table 2 and Figure 9).

Statistics report that the WorldView3 stereo dataset presents, as expected, the worst metrics due to the imaging geometry (Figure 10). Figure 9 on the other hand, show that higher errors are concentrated in vegetated areas (LiDAR and imagery are months apart), along the river surface and near building footprints.

Figure 11 shows a comparison of profiles in various urban contexts (an isolated building, very compact building blocks, and city blocks with large courtyards and separating roads). Results illustrate that with isolated blocks and sufficient object image coverage, a satisfying 3D geometry can be reconstructed with each of the tools tested (upper image). The advantage of a tri-stereo acquisition is evident only with wider spaces (lower figure), while no relevant differences can be found in the case of compact building blocks (middle image).

The GeoEye triplet was also processed as separate stereo-pairs, and the level of completeness of not-interpolated raster DSMs, derived with different tools (ERDAS and RSP), was compared. The completeness refers to the ratio between the matched points for the considered DSM and the maximum number of corresponding points of a specific DSM spacing grid (Aguilar et al., 2022). Table 3 and Figure 12 present these results: higher completeness levels are obtained using ERDAS, although it returned noisier results with respect to RSP. The pair-wise DSMs also highlight the role of imaging geometry (less favourable convergence angle for the FB combination) with respect to the completeness of the derived products.

Dataset	Type	Tool	Mean (m)	St. Dev. (m)
Geoeye	Triplet	RSP	0.117	6.919
		ERDAS	-0.241	6.652
WorldView3	Stereo	RSP	-2.992	9.118
		ERDAS	0.862	9.593
		Metashape	-1.951	10.998

Table 2. DSMs raster difference statistics: comparison between LiDAR ground truth and derived DSMs.

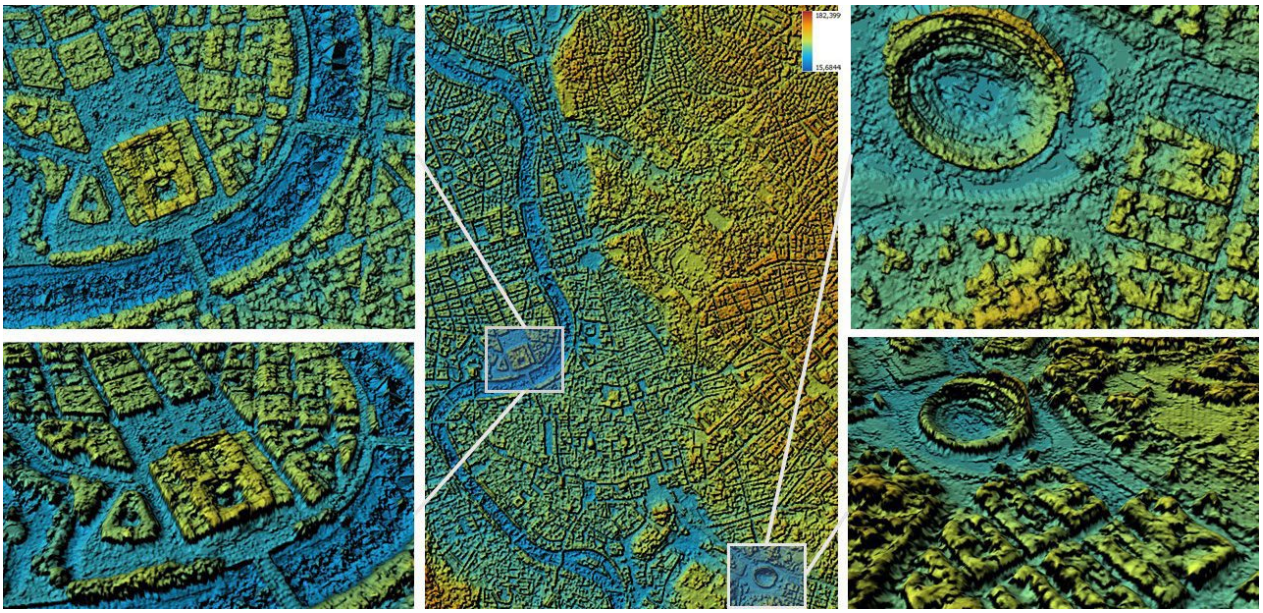

Figure 8: RSP's DSM derived from the GeoEye dataset over some about 5 x 7 km in Rome (Italy) and close views of the results.

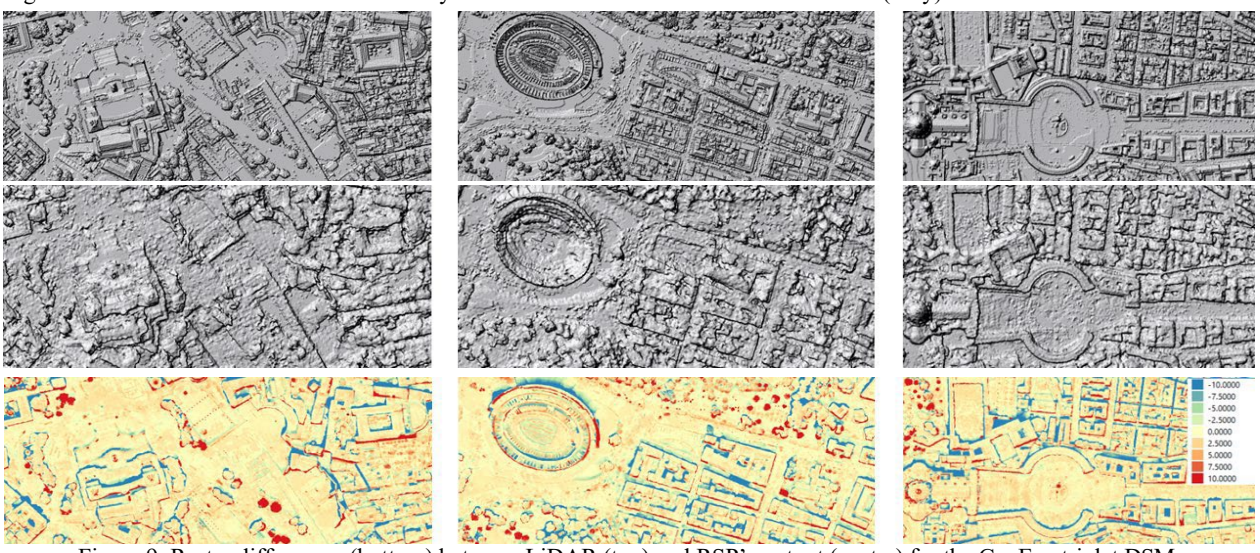

Figure 9. Raster differences (bottom) between LiDAR (top) and RSP's output (center) for the GeoEye triplet DSM.

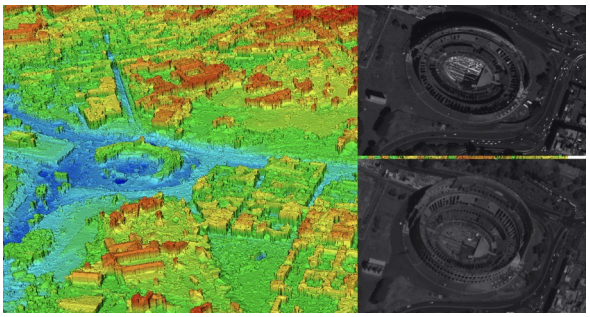

Figure 10: Resultant DSM for the WorldView-3 pair, with data voids due to the large viewing angles.

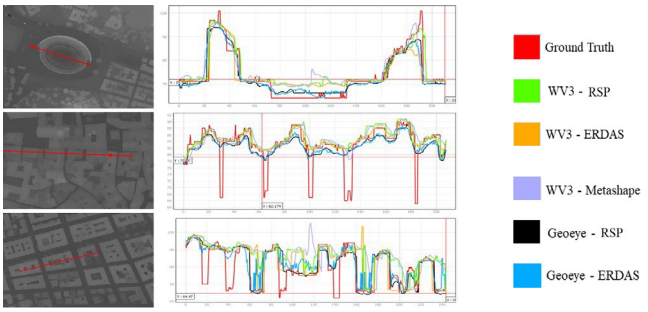

Figure 11. Comparisons of extracted profiles from DSMs of the two VHR Rome datasets processed with different tools.

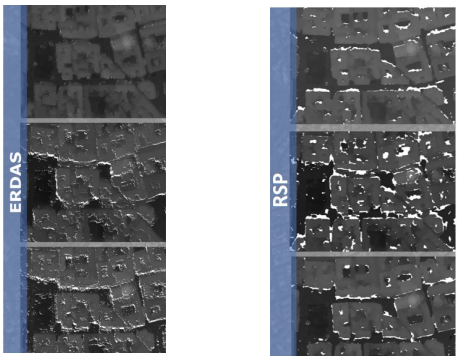

Figure 12. Level of completeness of non-interpolated raster DSMs derived from the GeoEye triplet stereo-pairs. From top to bottom: NB, FB, FN.

Pair	Angle	RSP	ERDAS
Forward-Nadir (FN)	15°	94.8%	99.0%
Nadir-Backward (NB)	14°	94.5%	94.9%
Forward-Backward (FB)	29°	88.6%	92.5%

Table 3: DSMs completeness analysis for the stereo processing of the GeoEye pairs over Rome. RSP uses a 1 pixel for left-right consistency check; using a higher threshold increases completeness.

5.2 GCPs influence in the processing workflow (Austrian datasets)

The use of GCPs in the image orientation phase helps to minimize georeferencing errors. The Austrian datasets capture a vast area of about 8 x 20 km over Allentsteig, featuring a primarily natural landscape with villages interspersed throughout. Previous studies have exploited these datasets to inspect their potential for DSMs production (Loghin et al., 2020) or for improving the VHR satellite image geometry (Loghin et al., 2022), leveraging the photogrammetric pipeline of Trimble Inpho. In our experimental analyses, we tested the processing capability of ERDAS and RSP: both datasets were processed, including available GCPs (Figure 13) and verifying the RMSE on selected Check Points (CPs) (Table 4).

Satellite	GCP/CP	$RMSE_x$ (m)	$RMSE_y$ (m)	$RMSE_z$ (m)
Pleiades	21/22	0.155	0.141	1.020
WorldView3	18/16	0.193	0.341	0.462

Table 4: RMSE [m] on Check Points (CPs) for both Austrian datasets (0.5m GSD).

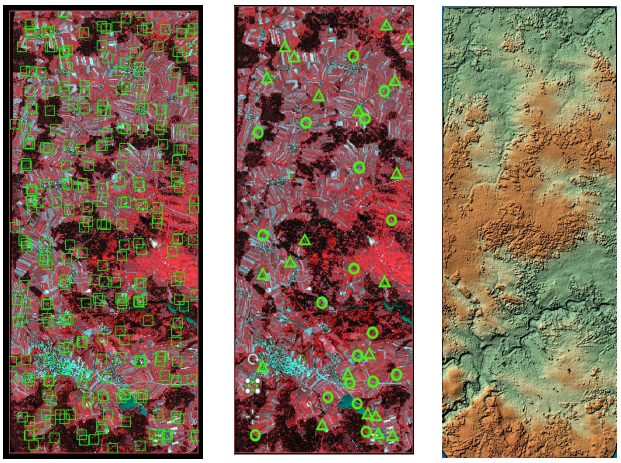

Figure 13: Distribution of automatically extracted tie points (left); used GCP (triangles) and CP (circles) for the RPC bias compensation (centre); generated DSM from WorldView-3.

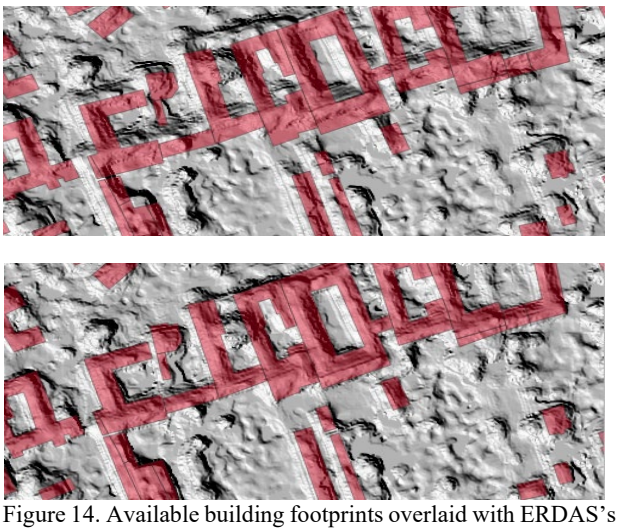

Figure 14. Available building footprints overlaid with ERDAS's DSM (WorldView3 triplet) without (top) and with (bottom) bias compensation.

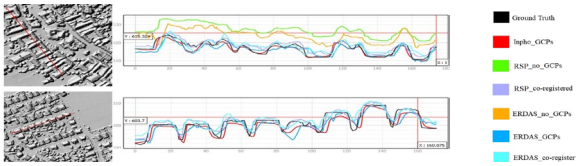

Figure 15. Profiles from the Pleiades DSMs with respect to ground truth. The figure below reports only the co-registered (and used for the analyses) results.

Both datasets were also processed without GCPs (reflecting a common scenario). After the co-registration with the available ground truth LiDAR data, the generated DSMs were overlaid with available vector topographic data to highlight possible shifts due to RPC bias (Figure 14). Profiles were also created (Figure 15), and excluding a vertical shift, the profile behaviours were consistent.

5.3 Assessing and visualizing sea and waterways (Dublin dataset)

The Pleiades triplet over Dublin covers a coastal area of approximately 10 x 10 km. The VHR images capture a portion of Dublin Bay, the river Liffey, and the waterways within the city. In order to minimize noise effects from water surfaces, a vector mask was created to exclude these areas from the study (Table 5). As no GCPs were used during the RPCs adjustment phase, the satellite-derive DSM and the available ground truth (Figure 16) were manually co-registered to remove horizontal and vertical shifts. Figure 17 shows a good correspondence between vector data and RSP's DSM.

Tool	Mean (m)	St. Dev. (m)
Metashape	-0.162	4.059
ERDAS	2.975	10.282
RSP	0.166	4.032

Table 5: DSMs raster difference statistics on the area of interest and by masking water surfaces in the DSMs.

Figure 17. Available topographic vector data overlaid on the generated DSM.

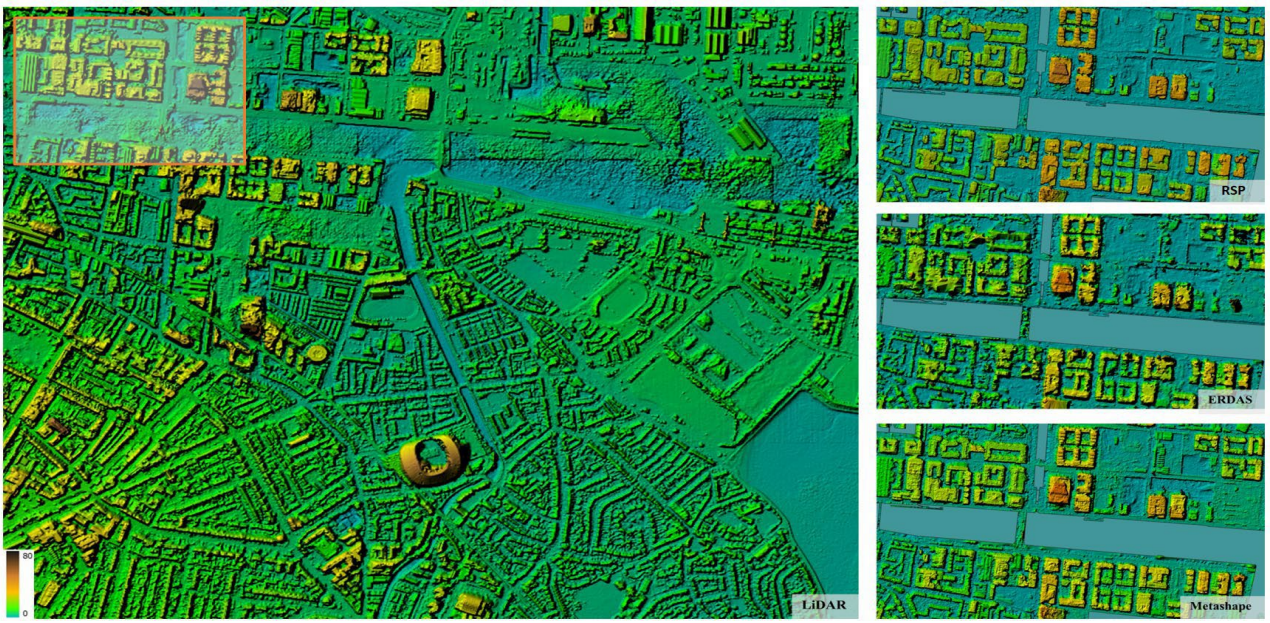

Figure 16: Data and results from the Dublin dataset (Pleaides triplet): ground truth data image-derived point cloud data (left) and some detailed views of DSMs generated with different tools (right).

5.4 3D reconstruction in a mountainous landscape (Trento datasets)

The Trento datasets include a valley (200 m a.s.l.) and the surrounding mountain area (up to 2000 m a.s.l.). The area covered extends to about 18 x 20 km in both cases. An example of the 3D reconstruction results with the RSP tool is shown in Figure 18. The DSMs from the GeoEye stereo-pairs were aligned to the LiDAR ground truth to evaluate the vertical accuracies (Table 6): two sub-areas of interest for further analyses (about 1,5 x 1 km) were selected in urban and mostly vegetated regions. The metric assessment shows similar results in the mean values in both cases and tools, while the larger standard deviation values could be due to the 3-year difference between LiDAR and satellite acquisitions.

The tri-stereo Pleiades dataset was exploited to test a framework for automated LOD2 model generation from DSM and orthophoto (Gui and Qin, 2021). The reconstruction results are presented in Figure 19 with good consistency between reference LiDAR and generated LOD2 building blocks.

	Urban		Vegetated	
	Mean (m)	St. Dev. (m)	Mean (m)	St. Dev. (m)
ERDAS	-1.021	7.421	-1.235	12.898
RSP	-1.024	7.433	-1.083	5.929

Table 6. Statistics [m] for the GeoEye DSMs considering urban and vegetated areas with respect to the LiDAR ground truth.

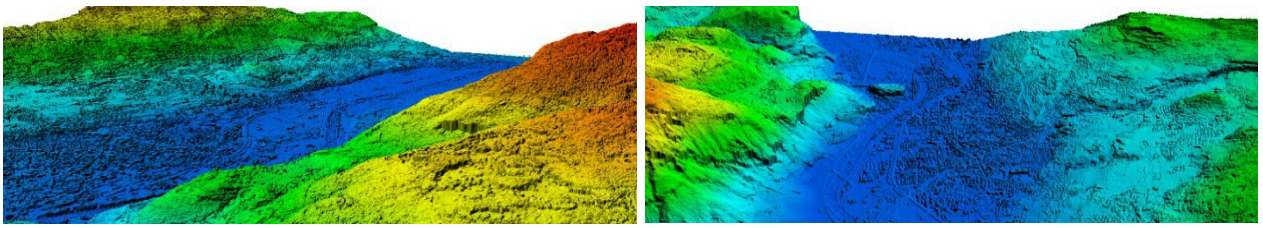

Figure 18: Color-coded RSP's DSM generated from the GeoEye dataset over Trento (GSD 0.5 m).

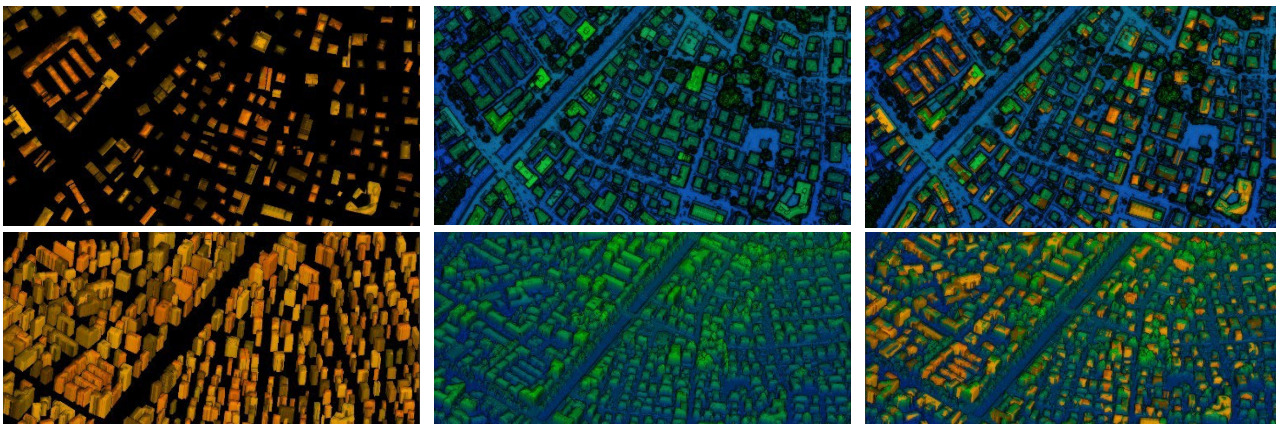

Figure 19: Automatic LoD2 reconstruction from satellite-based DSMs and orthophotos (left); reference DSM from LiDAR data (middle); overlapped data (right).

6. CONCLUSIONS

VHR satellite imagery is becoming increasingly of interest for NMCAs and other mapping and research institutions due to the clear advantage in providing regularly updated geospatial data (due to the high temporal resolution) and for the ability to map remote areas (weather-dependent).

This paper has presented various experimental tests and derived 3D data to investigate the potential of VHR satellite imagery for mapping needs. The work compared limitations of stereo pairs with respect to triplet datasets, the influence of GCPs in data processing, differences of 3D products in various landscape scenarios, and the potential for automatic LoD2 reconstruction from these data. The comparative analyses give examples, lessons learnt and an overview of the achievable quality of geospatial products that can be derived from these sources. In our experiments, different processing tools were used. It should be noted that experiments were performed using the default parameters of different software packages: tuning parameters of some of the software packages may produce different comparative results, such as completeness and smoothness of produced data. Results and analyses highlight a high potential and sufficient geometric correctness of these products in reconstructing and mapping areas in heterogeneous environments.

ACKNOWLEDGMENTS

The Allentsteig data were provided by the Institut fuer Militaerisches Geowesen (Vienna) within the ReKlaSat 3D research project. Dublin Pleiades datasets provided by European Space Agency under Third Party Mission license. Dublin 25cm DSM from 2017/2018 – from Ordnance Survey Ireland, 4km x 1.5km. The Trento images were purchased within the 3M project (co-founded Marie–Curie Actions FP7 – PCOFOUND – GA-2008-226070, acronym ‘‘Trentino Project’’).

REFERENCES

Aguilar, M.A., Nemmaoui, A., Aguilar, F.J. and Qin, R., 2019. Quality assessment of digital surface models extracted from WorldView-2 and WorldView-3 stereo pairs over different land covers. *GIScience & Remote Sensing*, Vol. 56(1), pp. 109-129.

Aguilar, M.A., Jiménez-Lao, R. and Aguilar, F.J., 2022. Assessment of Stereo-Extracted DSM from WORLDVIEW-3 Over Different Land Covers Depending on the Imaging Geometry. *ISPRS Ann. Photogramm. Remote Sens. Spatial Inf. Sci.*,Vol. *2*, pp. 31-38.

Agugiaro, G., Poli, D. and Remondino, F., 2012. Testfield Trento: Geometric evaluation of very high resolution satellite imagery. *The Int. Archives of the Photogrammetry, Remote Sensing and Spatial Information Sciences*, Vol. *39*, pp. 191-196.

Barbarella, M., Fiani, M. and Zollo, C., 2017. Assessment of DEM derived from very high-resolution stereo satellite imagery for geomorphometric analysis. *European J. Remote Sensing*, Vol. *50*(1).

Bosch, M., Kurtz, Z., Hagstrom, S., Brown, M., 2016. A Multiple View Stereo Benchmark for Satellite Imagery. Proc. *IEEE Applied Imagery Pattern Recognition Workshop* (AIPR).

Breaban, A.I., Oniga, V.E., Chirila, C., Loghin, A.M., Pfeifer, N., Macovei, M. and Nicuta Precul, A.M., 2022. Proposed Methodology for Accuracy Improvement of LOD1 3D Building Models Created Based on Stereo Pléiades Satellite Imagery. *Remote Sensing*, *14*(24), p. 6293.

Capaldo, P., Crespi, M., Fratarcangeli, F., Nascetti, A., Pieralice, F., Agugiaro, G., Poli, D., Remondino, F., 2012. DSM generation from optical and SAR high resolution satellite imagery: methodology, problems and potentialities. Proc. *IEEE Intern. Geoscience and Remote Sensing Symposium* (IGARSS).

De Franchis, C., Meinhardt-Llopis, E., Michel, J., Morel, J.-M., Facciolo, G., 2014. An automatic and modular stereo pipeline for pushbroom images. *ISPRS Ann. Photogramm. Remote Sens. Spatial Inf. Sci.*, 2.

Deilami, K. and Hashim, M., 2011. Very high resolution optical satellites for DEM generation: a review. *European Journal of Scientific Research*, *49*(4), pp. 542-554.

Denis, G., Claverie, A., Pasco, X., Darnis, J.P., de Maupeou, B., Lafaye, M., Morel, E., 2017. Towards disruptions in Earth observation? New Earth Observation systems and markets evolution: Possible scenarios and impacts. *Acta Astronautica*, Vol.137, pp. 415-433.

Di Rita, M., Nascetti, A. and Crespi, M., 2017. Open source tool for DSMs generation from high resolution optical satellite imagery: development and testing of an OSSIM plug-in. *International Journal of Remote Sensing*, *38*(7), pp. 1788-1808.

Dong, Y., Lei, R., Fan, D., Gu, L., Ji, S., 2020. A novel RPC bias model for improving the positioning accuracy of satellite images. *ISPRS Ann. Photogramm. Remote Sens. Spatial Inf. Sci.*, 2, pp. 35-41.

Dowman, I., Jacobsen, K., Konecny, G., Sandau, R., 2022. *High Resolution Optical Satellite Imagery*. Whittles Publishing.

Facciolo, G., de Franchis, C., Meinhardt, E., 2017. Automatic 3D reconstruction from multi-date satellite images. Proc. *IEEE CVPR*, pp. 1542–1551.

Fraser, C.S., Dial, G., Grodecki, J., 2006. Sensor orientation via RPCs. *ISPRS J. Photogrammetry and Remote Sensing*, Vol. 60, pp. 182-194.

Gao, J., Liu, J. and Ji, S., 2023. A general deep learning based framework for 3D reconstruction from multi-view stereo satellite images. *ISPRS J. Photogrammetry and Remote Sensing*, *195*, pp. 446-461.

Gui, S. and Qin, R., 2021. Automated LoD-2 model reconstruction from very-high-resolution satellite-derived digital surface model and orthophoto. *ISPRS J. Photogrammetry and Remote Sensing*, 181.

Hu, Y., Tao, V. and Croitoru, A., 2004. Understanding the rational function model: methods and applications. *Int. Archives of Photogrammetry and Remote Sensing*, *20*(6), pp. 119-124.

Junpeng, Y.U., Weidong, W.U., Jiaming, S.U.N., Yiyun, M.A.N. and Gang, S.H.E.N., 2022. A RFM adjustment method for satellite remote sensing image with Fourier compensation. *Acta Geodaetica et Cartographica Sinica*, *51*(1), p. 127.

Krauss, T., d'Angelo, P., Wendt, L., 2019. Cross-track satellite stereo for 3D modelling of urban areas. *European Journal of Remote Sensing*, Vol. 52(sup2), pp. 89-98.

Kuschk, G., d'Angelo, P., Qin, R., Poli, D., Reinartz, P., Cremers, D., 2014. DSM Accuracy Evaluation for the ISPRS Commision I Image Matching Benchmark. Int. Archives of the Photogrammetry, Remote Sensing & Spatial Information Sciences, Vol. 40(1), pp. 195-200.

Lebègue, L., Cazala-Hourcade, E., Languille, F., Artigues, S., Mele, O., 2020. CO3D - A worldwide one-meter accuracy DEM for 2025. *Int. Archives of the Photogrammetry, Remote Sensing and Spatial Information Sciences,* Vol. 43(B1), pp. 299-304.

Loghin, A.M., Otepka-Schremmer, J. and Pfeifer, N., 2020. Potential of Pléiades and WorldView-3 tri-stereo DSMs to represent heights of small isolated objects. *Sensors*, *20*(9).

Loghin, A.M., Otepka-Schremmer, J., Ressl, C. and Pfeifer, N., 2022. Improvement of VHR Satellite Image Geometry with High Resolution Elevation Models. *Remote Sensing*, *14*(10), p. 2303.

Luong, C.K. and Wolniewicz, W., 2005. Geometric models for satellite sensors. *Geodesy and Cartography*, *54*(4).

Marí, R., de Franchis, C., Meinhardt-Llopis, E., Anger, J. and Facciolo, G., 2021. A generic bundle adjustment methodology for indirect RPC model refinement of satellite imagery. *Image Processing on Line*, 11, pp. 344-373.

Partovi, T., Fraundorfer, F., Bahmanyar, R., Huang, H., Reinartz, P., 2019. Automatic 3-D building model reconstruction from very high resolution stereo satellite imagery. *Remote Sensing*, *11*(14), p. 1660.

Patil, S., Comandur, B., Prakash, T., Kak, A.C., 2019. A new stereo benchmarking dataset for satellite images. *arXiv preprint arXiv*:1907.04404.

Perko, R., Raggam, H. and Roth, P.M., 2019. Mapping with Pléiades - end-to-end workflow. *Remote Sensing*, *11*(17).

Poli, D. and Toutin, T., 2012. Review of developments in geometric modelling for high resolution satellite pushbroom sensors. *The Photogrammetric Record*, *27*(137), pp. 58-73.

Poli, D. and Caravaggi, I., 2013. 3D modeling of large urban areas with stereo VHR satellite imagery: lessons learned. *Natural Hazard*, Vol. 68, pp. 53-78.

Poli, D., Remondino, F., Angiuli, E., Agugiaro, G., 2015. Radiometric and geometric evaluation of GeoEye-1, WorldView-2 and Pléiades-1A stereo images for 3D information extraction. *ISPRS Journal of Photogrammetry and Remote Sensing*, Vol. 100, pp. 35-47.

Qin, R., 2016. Rpc stereo processor (rsp)–a software package for digital surface model and orthophoto generation from satellite stereo imagery. *ISPRS Ann. Photogramm. Remote Sens. Spatial Inf. Sci.,* 3.

Qin, R., 2019. A critical analysis of satellite stereo pairs for digital surface model generation and a matching quality prediction model. *ISPRS Journal of Photogrammetry and Remote Sensing*, Vol. 154, pp. 139-150.

Qin, R., Ling, X., Farella, E.M., Remondino, F., 2022. Uncertainty-Guided Depth Fusion from Multi-View Satellite Images to Improve the Accuracy in Large-Scale DSM Generation. *Remote Sensing*, 14(6).

Qin, R., Liu, T., 2022. A Review of landcover classification with very-high resolution remotely sensed optical images – Analysis unit, model scalability and transferability. *Remote Sensing*, 14(3), 646.

Reinartz, P., d'Angelo, P., Krauss, T., Poli, D., Jacobsen, K. and Buyuksalih, G., 2010. Benchmarking and quality analysis of DEM generated from high and very high resolution optical stereo satellite data. *The Int. Archives of the Photogrammetry, Remote Sensing and Spatial Information Sciences;* Vol. 38(1).

Rothermel, M., Gong, K., Fritsch, D., Schindler, K. and Haala, N., 2020. Photometric multi-view mesh refinement for high-resolution satellite images. *ISPRS Journal of Photogrammetry and Remote Sensing*, Vol.166, pp.52-62.

Rupnik, E., Pierrot-Deseilligny, M., Delorme, A., 2018. 3D reconstruction from multi-view VHR-satellite images in MicMac. *ISPRS Journal of Photogrammetry and Remote Sensing*, Vol. 139, pp. 201-211.

Shean, D.E., Alexandrov, O., Moratto, Z.M., Smith, B.E., Joughin, I.R., Porter, C. and Morin, P., 2016. An automated, open-source pipeline for mass production of digital elevation models (DEMs) from very-high-resolution commercial stereo satellite imagery. *ISPRS J. Photogrammetry and Remote Sensing*, *116*, pp. 101-117.

Sirmacek, B., Taubenböck, H., Reinartz, P., Ehlers, M., 2012. Performance Evaluation for 3-D City Model Generation of Six Different DSMs From Air- and Spaceborne Sensors. *IEEE J. of Selected Topics in Applied Earth Observations and Remote Sensing*, Vol.5(1), pp. 59-70.

Stylianidis, E., Akca, D., Poli, D., Hofer, M., Gruen, A., Sanchez, Martin, S., Smagas, K., Walli, A., Altan, O., Jimeno E., Garcia, A., 2020. FORSAT: A 3D forest monitoring system for cover mapping and volumetric 3D change detection. *Int. Journal of Digital Earth*, Vol. 13(8).

Stucker, C., Ke, B., Yue, Y., Huang, S., Armeni, I., Schindler, K., 2022. Implicity: city modeling from satellite images with deep implicit occupancy fields. *ISPRS Ann. Photogramm. Remote Sens. Spatial Inf. Sci.,* V-2-2022, pp. 193-201.

Tang, S., Wu, B. and Zhu, Q., 2016. Combined adjustment of multi-resolution satellite imagery for improved geo-positioning accuracy. *ISPRS J.Photogrammetry and Remote Sensing*, 114.

Xiong, Z., Zhang, Y., 2009. A Generic Method for RPC Refinement Using Ground Control Information. *PE&RS*, Vol. 75(9), pp. 1083-1092.

Watson, C.S., Elliott, J.R., Amey, R.M.J., Abdrakhmatov, K.E., 2022. Analyzing Satellite-Derived 3D Building Inventories and Quantifying Urban Growth towards Active Faults: A Case Study of Bishkek, Kyrgyzstan. *Remote Sensing*, 14, 5790.